Remote Sensing Applications: Society and Environment 26 (2022) 100770

Contents lists available at ScienceDirect

Remote Sensing Applications: Society and Environment

journal homepage: www.elsevier.com/locate/rsase

Flash drought identification from satellite-based land surface water index

Jordan I. Christian [a,*], Jeffrey B. Basara [a,b], Lauren E.L. Lowman [c], Xiangming Xiao [d], Daniel Mesheske [b], Yuting Zhou [e]

[a] School of Meteorology, University of Oklahoma, Norman, OK, USA
[b] School of Civil Engineering and Environmental Science, University of Oklahoma, Norman, OK, USA
[c] Department of Engineering, Wake Forest University, Winston-Salem, North Carolina, United States
[d] Department of Microbiology and Plant Biology, Center for Earth Observation and Modeling, University of Oklahoma, Norman, OK, USA
[e] Department of Geography, Oklahoma State University, OK, USA

A B S T R A C T

Flash droughts can lead to significant agricultural and ecosystem impacts via rapid land surface desiccation. While gridded weather and climate datasets, land surface models, or widely spaced in situ observations are typically used to quantify flash drought development, coarse spatial data limits the ability to determine fine-scale spatial evolution of flash drought at landscape and ecosystem scales. In this study, a novel approach is introduced to objectively identify flash drought using the land surface water index (LSWI) derived from satellite observations. LSWI is a water-related vegetation index that represents the total water content in vegetation by using the near-infrared and shortwave infrared bands. LSWI was derived from the Moderate Resolution Imaging Spectroradiometer (MODIS) Terra surface reflectance (MOD09A1) with a 500 m spatial resolution and an 8-day temporal resolution. When applied to two well-established case studies, LSWI anomalies were able to capture the temporal and spatial evolution of flash drought over Oklahoma during the years of 2011 and 2012. In addition, rapid changes of LSWI during flash drought were comparable across space and time to the reanalysis-based Standardized Evaporative Stress Ratio (SESR), while negative anomalies of LSWI following flash drought corresponded with drought impacts via the United States Drought Monitor. It was found that LSWI was able to identify flash drought with a finer spatial resolution (500 m) and revealed spatial propagation of flash drought events that would not otherwise be seen with coarser meteorological data (e.g., ~32 km at the lowest latitude for the North American Regional Reanalysis data). Furthermore, LSWI greatly enhanced the ability to detect rapid changes in surface conditions driven by flash drought and was able to provide early warning for drought development when compared with the USDM across Oklahoma. As such, the temporal and spatial evolution of flash drought depicted by LSWI and the presented methodology improves our ability to identify flash drought at high spatial resolution using satellite remote sensing and detect rapid changes in surface conditions. In light of these results, the novel LSWI approach demonstrates that satellite remote sensing applications using an objective technique are advantageous for flash drought detection in near real-time and at fine spatial scales.

1. Introduction

Drought is a complex phenomenon that develops from a diverse set of drivers and contributes to a wide range of socioeconomic impacts (Basara et al., 2013). Fundamentally, drought develops during a given period of below-average rainfall and are often characterized by slow development on seasonal timescales (Wilhite et al., 2007). However, if precipitation deficits are accompanied by above average evaporative demand (higher temperatures, increased vapor pressure deficit, and surface insolation), rapid drought intensification (i.e., flash drought) can occur (Otkin et al. 2013, 2018; Lisonbee et al., 2021). Flash drought events accelerate negative outcomes experienced at the land surface via rapid depletion of available soil water and excessive moisture stress on vegetation.

* Corresponding author. School of Meteorology, University of Oklahoma, Norman, OK, USA.
E-mail address: jchristian@ou.edu (J.I. Christian).

https://doi.org/10.1016/j.rsase.2022.100770
Received 20 September 2021; Received in revised form 8 March 2022; Accepted 30 April 2022
Available online 4 May 2022

Further, flash drought development can ultimately result in significant agricultural losses (Jin et al., 2019), increased frequency in wildfires (Hoell and Coauthors, 2020), and promote the development of heatwaves via land-atmosphere interactions (Christian et al., 2020).

Flash drought can occur over a wide range of ecosystems and climate types, except in areas that are too arid to produce a significant change in soil moisture when a lack of precipitation occurs (Koster et al., 2019). Specifically over the United States, flash droughts occur most often over the central United States and have preferential occurrence over land cover types associated with grasslands and agricultural production (Christian et al. 2019a, 2021). Furthermore, flash droughts are most likely to occur during the middle of the growing season across the central United States when evaporative demand is at its peak (Chen et al., 2019; Christian et al., 2019b, Otkin and Coauthors, 2021). The onset of flash drought can spatially propagate across a large region throughout the growing season (e.g., the central United States flash drought in 2012; Basara et al., 2019), but also can occur concurrently over a region when the large-scale atmospheric conditions conducive for flash drought development persist (e.g., the flash drought over southwestern Russia in 2010; Christian et al., 2020).

Within the scientific literature, flash droughts have primarily been evaluated by one of three groups of variables: soil moisture, evaporative demand, and evaporative stress (Lisonbee et al., 2021). Soil moisture is a commonly used variable for flash drought detection as rapid decreases in soil moisture can depict flash drought development, and limited soil water content represents critical impacts from drought conditions (Ford and Labosier, 2017; Yuan et al., 2019; Osman et al., 2021). Evaporative demand has also been used for examining flash drought (Hobbins et al., 2016; McEvoy et al., 2016, Pendergrass and Coauthors, 2020) given that increasing evaporative demand will concurrently increase evapotranspiration leading to a rapid depletion of soil moisture. The last metric often used in flash drought analysis is stress-based and is derived using the ratio between actual evapotranspiration and potential evapotranspiration to represent the overall moisture stress on the environment (Basara et al., 2019; Otkin et al. 2013, 2014; Nguyen et al., 2019). Rapid increases in evaporative stress can detect flash drought development, while large values of evaporative stress (low actual evapotranspiration and high potential evapotranspiration) indicate desiccation of the land surface and vegetative impacts. Two versions of evaporative stress have been used for flash drought: the satellite-based evaporative stress index (ESI; Anderson et al., 2007a; Anderson et al., 2007b) and the standardized evaporative stress ratio (SESR; Christian et al., 2019a).

In addition to studies that have utilized the satellite-based ESI to explore rapid drought intensification (Otkin et al., 2013), other satellite observations have also be used to investigate flash drought development. For example, satellite-based evapotranspiration and solar-induced chlorophyll fluorescence have been used to assess the impact of the 2017 flash drought across the United States Northern plains (He et al., 2019), while leaf area index and gross primary productivity have quantified terrestrial carbon dynamics over China (Zhang et al., 2020). While satellite observations have been used to explore land surface characteristics during flash drought, a knowledge gap remains to leverage satellite data for objective flash drought identification.

Satellite remote sensing can provide additional insight into the impacts of flash drought development through targeted observations focused on vegetation indices (VIs). As vegetation states reflect responses to atmospheric and soil water stress (Lowman and Barros 2018), VIs can be interpreted as aggregates of both types of drying conditions. Further, VIs have the potential to identify simultaneously the rapid intensification towards drought and deteriorating land surface conditions in the same metric at higher spatial resolutions (e.g., 250 m, 500 m, 1 km) than other non-VI metrics currently used for flash drought identification (e.g., 5–50 km; Basara et al., 2019; Koster et al., 2019; Zhang et al., 2018). As such, vegetation-based flash drought detection may reveal the evolution of flash drought at finer spatial scales than the broader flash drought development identified via land surface models and gridded datasets with coarser spatial resolutions.

Several different VIs derived from remote sensing data exist for monitoring vegetation health. Two of the most commonly used VIs include the Normalized Difference Vegetation Index (NDVI) and Enhanced Vegetation Index (EVI). The NDVI and EVI detect the apparent greenness of the land surface and provide an assessment of where the vegetation canopy is in its growing season (Xue and Su 2017). However, water-related VIs also exist and are able to represent the total water content in vegetation by using the near-infrared (NIR) and shortwave infrared (SWIR) bands. The SWIR spectral band provides a measurement of moisture and is negatively related to leaf water content (Tucker 1980), while the NIR spectral band acts as a moisture reference (Bajgain et al., 2017). While VIs that use a combination of the NIR and SWIR bands have been referenced with different names, the commonly used naming convention for this combination of bands is the Land Surface Water Index (LSWI; Xiao et al., 2002; Xiao et al., 2004; Chandrasekar et al., 2010). LSWI has been used to identify drought conditions and has a higher sensitivity to developing drought compared to the NDVI and EVI (Bajgain et al. 2015, 2017; Chandrasekara et al., 2011, Wagle and Coauthors, 2014, Zhou and Coauthors, 2017). Additionally, LSWI has been used to assess the effect of water-stress on photosynthesis in the Vegetation Photosynthesis Model (Xiao et al., 2004; Dong and Coauthors, 2015; Zhang et al., 2017).

Because the LSWI has been shown to have a high sensitivity to the severity of drought, we hypothesize that this VI may be used to identify regions undergoing rapid drought development. Thus, the purpose of this study is to determine the utility of satellite remote sensing specifically for flash drought identification via an objective methodology. Case study analysis of known flash drought events across Oklahoma are used to 1) investigate the spatial and temporal evolution of flash drought depicted by the LSWI, 2) compare flash drought identification derived by LSWI with flash drought derived from an evaporative stress metric (SESR), and 3) examine the spatiotemporal relationship of developing drought conditions represented by the LSWI and the United States Drought Monitor (USDM). Ultimately, this study investigates the suitability of objectively identified flash drought via LSWI, as well as the advantages and limitations of using satellite observations for flash drought depiction.

2. Data and methods

2.1. Study domain

To examine the utility of satellite remote sensing for flash drought detection, Oklahoma was selected as the region of focus for this study as large areas within Oklahoma have experienced rapid drought intensification during notable flash drought years. These include the well-known flash drought events across the central United States in 2012 (Basara et al., 2019; DeAngelis et al., 2020; Jin et al., 2019, Otkin and Coauthors, 2016) and flash drought development across Oklahoma in 2011 (Ford et al., 2015; Otkin et al., 2013). Further, Oklahoma contains many different land cover types, including grasslands (59.9% of land area), savannas (15.1%) croplands (14.7%), and forests (3.3%; Fig. 1). This diversity of land cover types also presents an opportunity to explore the utility of flash drought detection using VIs across different ecosystems. Lastly, it is important to note that flash drought identification was focused on the approximate growing season across Oklahoma between March and September.

2.2. Reanalysis data and the USDM

Satellite-derived flash drought identification was compared to reanalysis-based flash drought identification to examine the temporal and spatial relationships between vegetation desiccation and rapid drought intensification depicted by evaporative stress. The meteorological perspective of flash drought development was analyzed using SESR (Christian et al., 2019a); SESR is calculated by standardizing the ratio between evapotranspiration (ET) and potential evapotranspiration (PET) at pentad intervals and has previously identified flash drought development across the Southern Great Plains during 2011 and 2012 (Basara et al., 2019; Christian et al., 2019a), climatological flash drought across the United States (Christian et al., 2019b; Osman et al., 2021), and land surface impacts due to flash drought (vegetation health and land surface desiccation; Christian et al., 2020). Negative values of SESR indicate greater evaporative stress on the environment, while positive values of SESR indicate reduced evaporative stress. Consistent with previous studies focused on the study domain that identified flash drought development across the Southern Great Plains during 2011 and 2012 (Basara et al., 2019; Christian et al., 2019a), the North American Regional Reanalysis (NARR; Mesinger and Coauthors, 2006) dataset was used to provide ET and PET between 1979 and 2020. While the NARR has been used in previous flash drought studies and has been shown to identify flash drought across the Southern Great Plains, it is important to note that different reanalysis datasets may produce different locations and timing of flash drought development depending on the land surface model used. SESR computed from NARR data provides a reference point for evaporative stress derived flash drought and it's comparison to VI-based flash drought. However, the overarching purpose of this study is to develop an objective flash drought methodology utilizing satellite observations.

Drought conditions from the USDM were also used to examine the timing and severity of drought development depicted by the LSWI. The USDM uses a "convergence of evidence" approach to objectively identify drought using several climatological inputs, as well as the incorporation of local expert reports of land surface conditions (Svoboda and Coauthors, 2002). Further, the USDM is often used for comparison in flash drought verification studies (Anderson et al., 2013; Christian et al., 2019a; Ford et al., 2015; Otkin et al., 2013). For areal averages in this study, drought categories (D0-D4) are converted to integer equivalents (0–4), while non drought conditions are represented by −1.

2.3. Satellite observations

To quantify flash drought development using a satellite-based approach, the Land Surface Water Index (LSWI) was calculated for the period spanning 2001–2020. LSWI has been shown to have a greater sensitivity to drought development in the study domain compared to other commonly used VIs such as the NDVI and EVI (Bajgain et al., 2015). LSWI is given as:

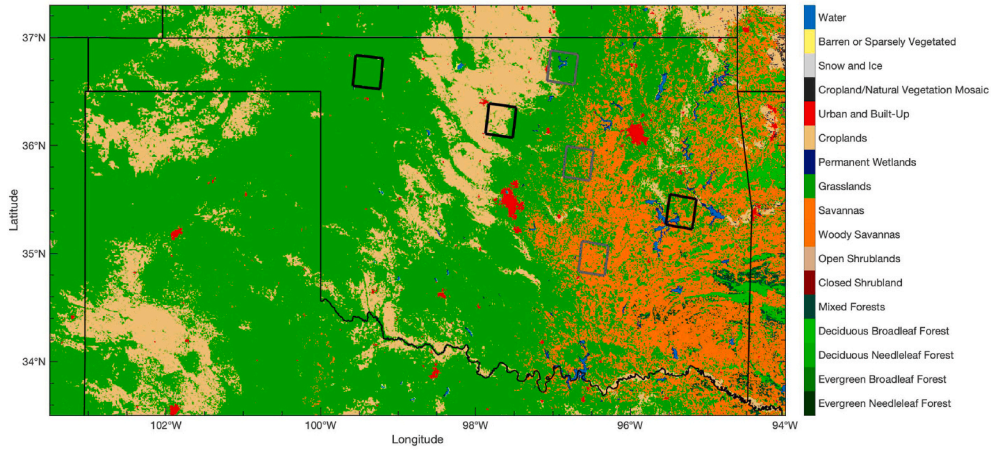

Fig. 1. Land cover type from MODIS version 6 (MCD12Q1) for 2012 in Oklahoma using the International Geosphere Biosphere Programme classification. The black rectangles outline the grid cells used for analysis in Fig. 6, and the gray rectangles outline the grid cells used for analysis in Fig. 7.

$$LSWI = \frac{\rho_{858} - \rho_{1640}}{\rho_{858} + \rho_{1640}}$$

where ρ_{858} and ρ_{1640} is the percentage of reflected radiation in the NIR band at 858 nm and the SWIR band at 1640 nm, respectively. LSWI was derived from the Moderate Resolution Imaging Spectroradiometer (MODIS) Terra surface reflectance (MOD09A1) and has a 500 m spatial resolution with an 8-day temporal resolution. For time series analysis, LSWI was standardized for each 8-day period using the climatological data from 2001 to 2020. Negative values of standardized LSWI indicate below-average water content in vegetation, while positive values indicate above-average water content in vegetation.

2.4. Processing climatological LSWI

Key to flash drought identification is the ability to quantify percentiles or normalized values from a climatology of data (e.g., 20 years of data). As such, a continuous dataset with minimal interruption in data availability is required. Such data consistency is particularly challenging with satellite observations given pixels can be contaminated due to cloud coverage or frozen precipitation covering the land surface. In order to prepare a high-quality dataset of LSWI for the analysis, we followed the method proposed by Chen et al. (2004) which consists of masking contaminated and poor quality pixels, applying a linear interpolation in time to fill missing values, and apply a Savitzky-Golay filter to smooth noise associated with cloud contamination and atmospheric variability.

To prepare a climatological dataset of LSWI, pixels were masked for clouds, snow/ice coverage, and locations over water. In addition, pixels were masked where band 2 (NIR) and band 6 (SWIR) did not pass quality control according to band quality data provided in MOD09A1. Data availability of LSWI across Oklahoma and the surrounding Southern Great Plains following the masking procedure for pixels is shown in Fig. 2a. Within the domain and at this preliminary step in data preparation, only 5.9% of pixels yielded data availability exceeding 99% between 2001 and 2020 during the growing season (March through September). Further, a majority of the pixels had available data between 94% and 99%, which corresponds to approximately 1–2 missing 8-day periods per year in the growing season. Given only 28 total 8-day periods of satellite data exist per growing season (March through September), even a few missing temporal periods can severely limit identification of flash drought events. As such, it was critically important to increase the percentage (e.g., close to 100%) of useable climatological data for a comprehensive analysis of flash drought.

To account for masked satellite data, LSWI was linearly interpolated on a pixel-by-pixel basis. For example, if a pixel located at 36°N and 98°W was masked for July 12, 2001, LSWI at that pixel location for July 4, 2001 and July 20, 2001 was averaged to produce an LSWI value for 12 July. A visual example of this process across the entire domain is shown in Fig. 3 for May 25, 2005. After the cloud mask was applied, a large portion of eastern Oklahoma yielded unavailable data for the study (Fig. 3b). However, after the linearly interpolated data computed from May 17, 2005 (Figure 3a) and June 2, 2005 (Fig. 3c) was added, nearly all of the masked data in Fig. 3b was filled in (Fig. 3d). Linear interpolation was also used to fill masked data at pixels with two or more consecutive time steps of masked data. A limitation of interpolating two or consecutive time steps is that rapid declines that may have been otherwise present in quality controlled LSWI data will be smoothed out over several time periods. This may limit identification of flash drought for situations where several consecutive data periods are masked. However, across the domain and in the growing season, pixels had two or more consecutive masked time steps occur twice on average during the 20 years of data, with a median of one occurrence per pixel. As

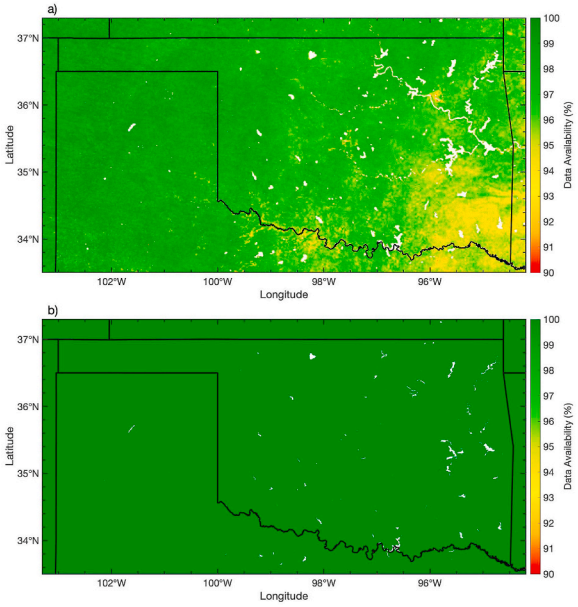

Fig. 2. Data availability of LSWI during the growing season (March through September) from 2001 to 2020 a) prior to linear interpolation and b) after linear interpolation.

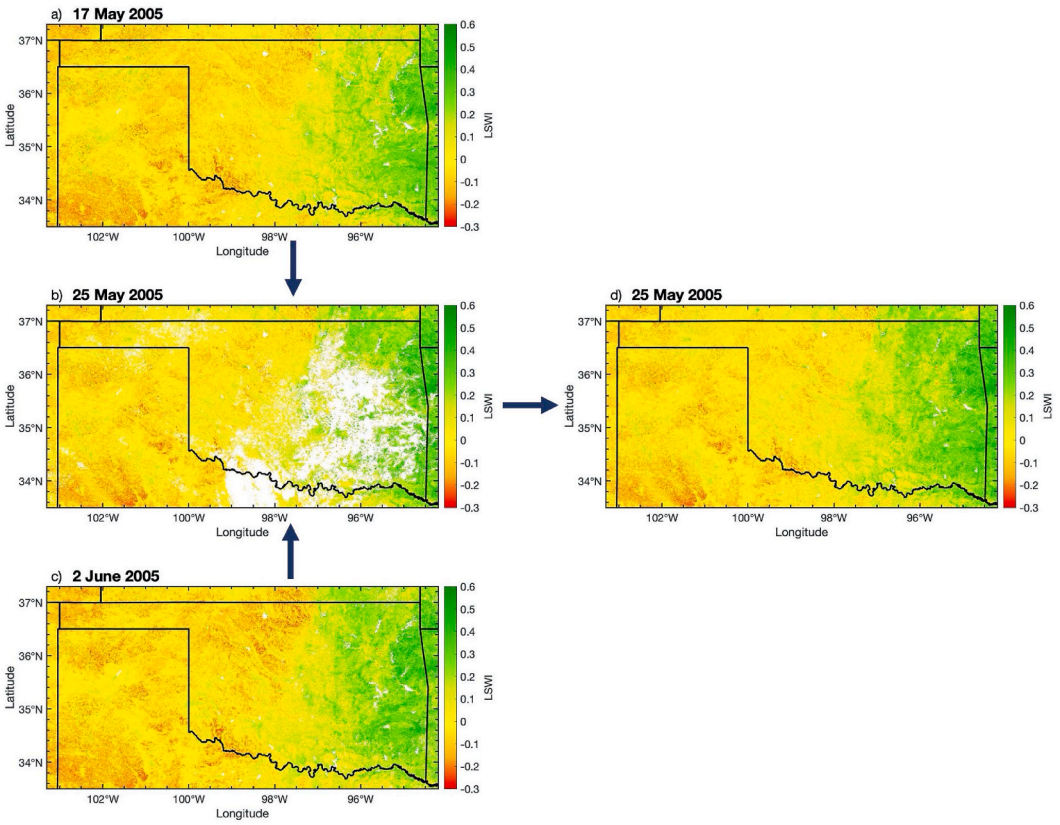

Fig. 3. Example of linear interpolation to gap-fill masked LSWI data. May 25, 2005 contains masked LSWI data (b), and LSWI data from May 17, 2005 (a) and June 2, 2005 (c) are used to fill in masked data for May 25, 2005 (d).

such, the occurrence of two or more consecutive masked pixels was very rare (less than 0.2% of the time) and would have minimal impact on flash drought detection via LSWI. In addition, the Savitzky-Golay filtering procedure discussed in the following section assists in retaining rapid changes in LSWI data that may have been smoothed out during the process of linear interpolation with two or more consecutive masked time steps. Once the interpolation process was applied for all time steps and pixels between 2001 and 2020, data availability increased to 100% across Oklahoma and the surrounding Southern Great Plains (Fig. 2b).

While MODIS surface reflectance and interpolation can provide a continuous dataset of LSWI both spatially and temporally, artifacts in the retrieval process from MODIS can create noise in the time-series of LSWI. These disturbances in data retrieval are a result of aerosols, water vapor, cloud contamination, and bi-directional effects (Cihlar et al., 1997). To account for these effects on LSWI, the method presented in Chen et al. (2004) is used to smooth the data and impute missing values in a way that preserves the seasonality of spectral retrievals. The Chen et al. (2004) method uses the Savitzky-Golay filter (Savitzky and Golay, 1964) to remove noise while preserving higher moments in the data. Filtering methods, such as the Savitzky-Golay filter, are crucial when smoothing LSWI for flash drought analysis, as large sub-seasonal declines in LSWI during flash drought events are preserved during the filtering process. Following the outline in Chen et al. (2004), LSWI was filtered in a three-step process at each pixel in the dataset:

1. Use the Savitzky-Golay filter on the original LSWI time-series ($LSWI^0$) to produce a new time-series ($LSWI^{SG1}$).
2. Generate a new time-series ($LSWI^1$) by replacing values in $LSWI^0$ with $LSWI^{SG1}$ where $LSWI^0$ is less than $LSWI^{SG1}$.
3. Use the Savitzky-Golay filter on $LSWI^1$ to produce the final time-series of LSWI.

For the use of the Savitzky-Golay filter in steps 1 and 3, $d = 4$ was used for the degree of polynomial, and $m = 6$ was used as the half-width of the smoothing window (Chen et al., 2004). After this process, a final time-series of LSWI is produced that smooths the time-series, increases values in the LSWI time-series profile to approach the "true" LSWI time-series profile, and preserves sub-seasonal fluctuations in LSWI.

2.5. Flash drought identification

Flash drought was identified via LSWI (referred to as FD_LSWI; Fig. 4) and SESR (referred to as FD_SESR) via a flash drought identification methodology adopted from Christian et al. (2019a) which has previously been used for flash drought case studies (Basara et al., 2019; Christian et al., 2020) and climatological analyses (Christian et al., 2019b; Osman et al., 2021). FD_SESR includes four criteria, with two criteria emphasizing environmental impact and two additional criteria focused on the rapid rate of intensification

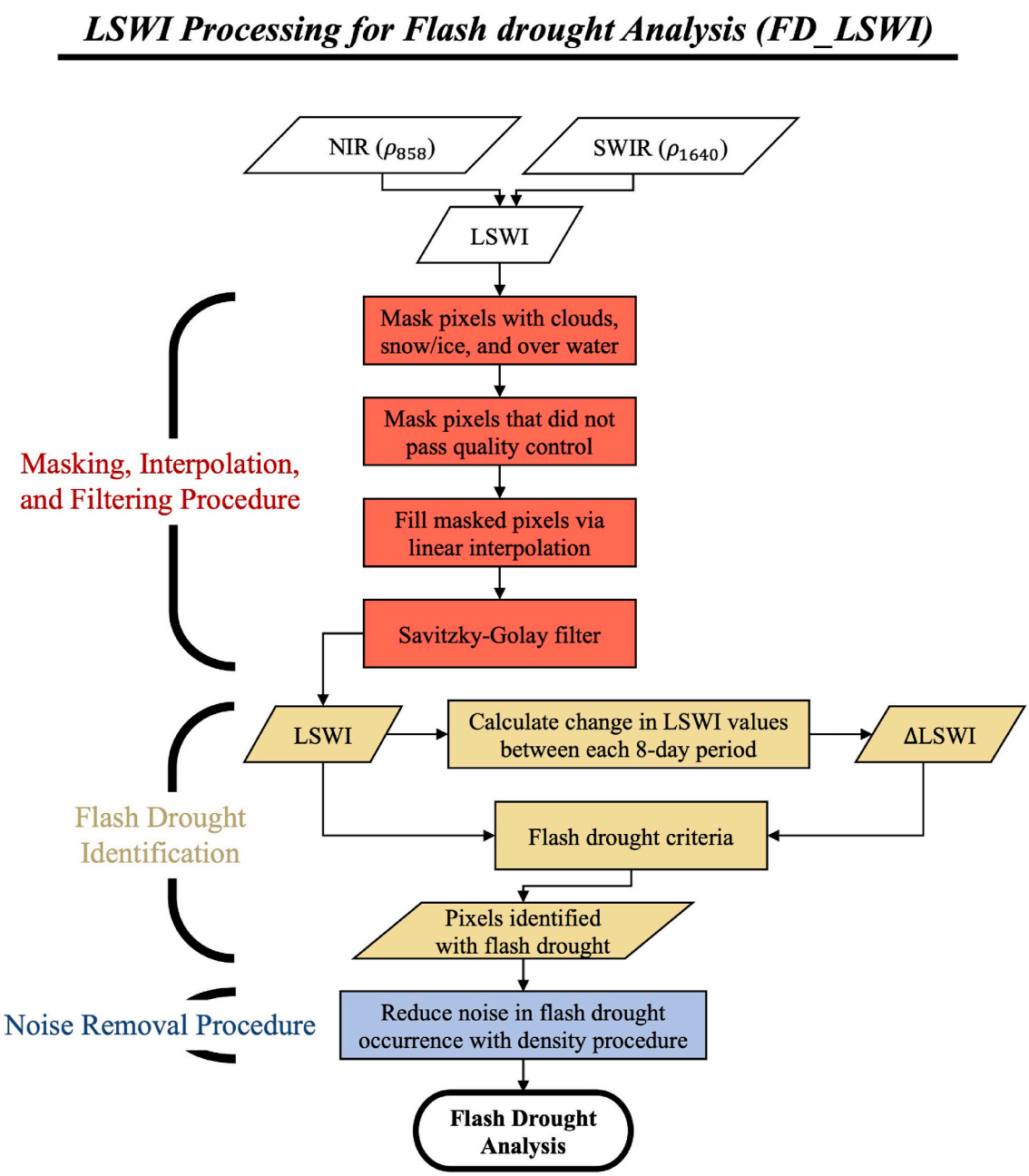

Fig. 4. A flowchart of the FD_LSWI process for calculating LSWI including 1) masking, interpolation, and filtering, 2) identifying flash drought, and 3) removing noise.

toward drought. For SESR and the pentad-to-pentad change in SESR (referred to as ΔSESR), the criteria are summarized as:

1. a minimum length of 30 days
2. a final SESR value below the 20th percentile
   3a. ΔSESR must be at or below the 40th percentile
   3b. no more than one ΔSESR above the 40th percentile following a ΔSESR that meets criterion 3a
4. the mean change in SESR during the entire length of the flash drought must be less than the 25th percentile.

For all percentile values used in criteria 2 and 3, percentiles are utilized from the distribution of SESR and ΔSESR at local grid cells (pixels) and specific time steps for all years available in the dataset. For criterion 4, percentiles are calculated from the distribution of ΔSESR at local grid cells for time steps that are encompassed within the flash drought event.

Given the additional filtering and smoothing provided for LSWI, FD_LSWI uses a simplified version of the FD_SESR methodology that uses only three criteria. In the updated methodology, criteria 1 and 2 remain the same, but criteria 3 and 4 are merged into a

simplified criterion to identify the rapid intensification of drought. This refined methodology using LSWI and ΔLSWI (change in 8-day periods of LSWI) is given as:

1. a minimum length of 32 days
2. a final LSWI value below the 20th percentile
3. ΔLSWI below the 25th percentile at each time step

A flash drought event ends when criteria 3 in FD_LSWI is no longer satisfied. Criteria 3 and 4 from the FD_SESR methodology can be simplified to criterion 3 in the FD_LSWI as criteria 3 and 4 from FD_SESR were created to account for pentad-to-pentad volatility in the SESR flash drought framework. With the smoothing technique from Chen et al. (2004) applied to LSWI, the conjunctive use of criteria 3 and 4 in FD_SESR are no longer needed, and can be reduced to a simple criterion to identify rapid drought development. In addition, a minor modification is made to criterion 1 for LSWI. Because SESR is provided in pentads, criterion 1 is divisible by 5-day periods such that a period of rapid drought intensification must be at least 6 total pentads long to qualify as a flash drought event. However, LSWI is provided in 8-day composites. As such, It is also important to note that the flash drought development window between FD_SESR and FD_LSWI may be offset by up to three days solely due to the discrepancy of temporal resolutions between FD_SESR (5-day periods) and FD_LSWI (8-day periods). However, any temporal comparisons made in this study regarding flash drought are primarily focused on multi-week differences between the two approaches (VI vs. evaporative stress), and timing differences due to in temporal resolution (up to three days) are negligible.

2.6. *Processing LSWI-derived flash drought*

An artifact of high-resolution flash drought analysis using 500 m pixels is that sporadic pixels indicating rapid drought intensification create challenges in identifying coherent areas that display consistent and concurrent flash drought development. To illustrate the impact of the masking process on flash drought identification, an example is shown from 2003 across Oklahoma (Fig. 5). Initial results directly from the flash drought identification process reveal areas with various pixel densities displaying flash drought occurrence but strong spatial coherence of flash drought remains difficult to determine (Fig. 5a).

To emphasize areas with the highest density of pixels identified with flash drought, a 20 km^2 spatial box was first centered over each pixel in the domain. A pixel was masked for flash drought development if the density of pixels with flash drought in the 20 km^2 spatial box was less than 25% of all pixels contained in the spatial box. The 20 km^2 size for the spatial box was selected to match similar spatial resolutions in previous flash drought studies (e.g., 5 km–50 km; Basara et al., 2019, Christian et al., 2020, Koster et al., 2019, Otkin and Coauthors, 2016, Zhang et al., 2018). The 25% threshold was selected to reduce some of the "noise" of flash drought variability at high-resolution while still maintaining the broader signal of flash drought development. However, it is important to note that lowering the density threshold (less than 25%) will reveal more flash drought pixels and subsequently more "noise", while raising the density threshold (more than 25%) will refine strong flash drought signals with the consequence of removing the broader flash drought signal of occurrence.

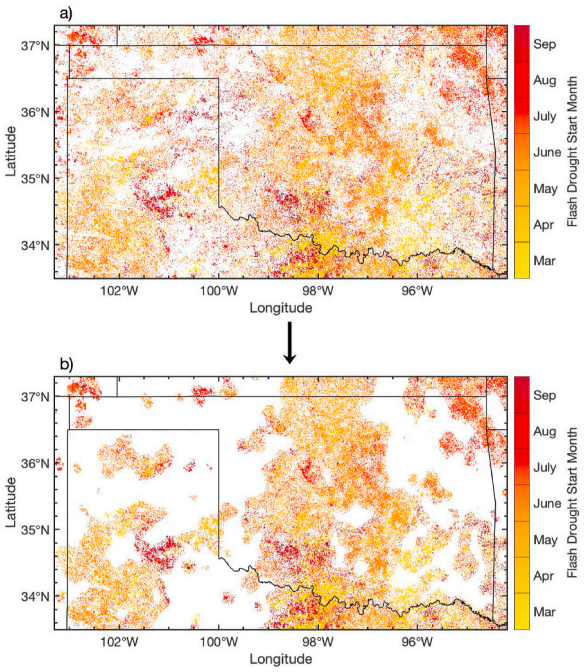

Fig. 5. Illustration of flash drought processing for 2003. The top panel (a) shows flash drought pixels from the identification methodology and the bottom panel (b) shows the regions undergoing flash drought development after masking out areas with a low density of pixels with flash drought.

Following the noise removal process, the resulting spatial extent of flash drought development for 2003 across Oklahoma is shown in Fig. 5b. Overall, a north-south swath of flash drought occurred across central Oklahoma, with flash drought occurrence later in the growing season across far northeast Oklahoma. Ultimately, this process was used to reveal spatial signals in flash drought occurrence that would otherwise be challenging to depict with raw, remotely-sensed flash drought data via LSWI (Fig. 5a).

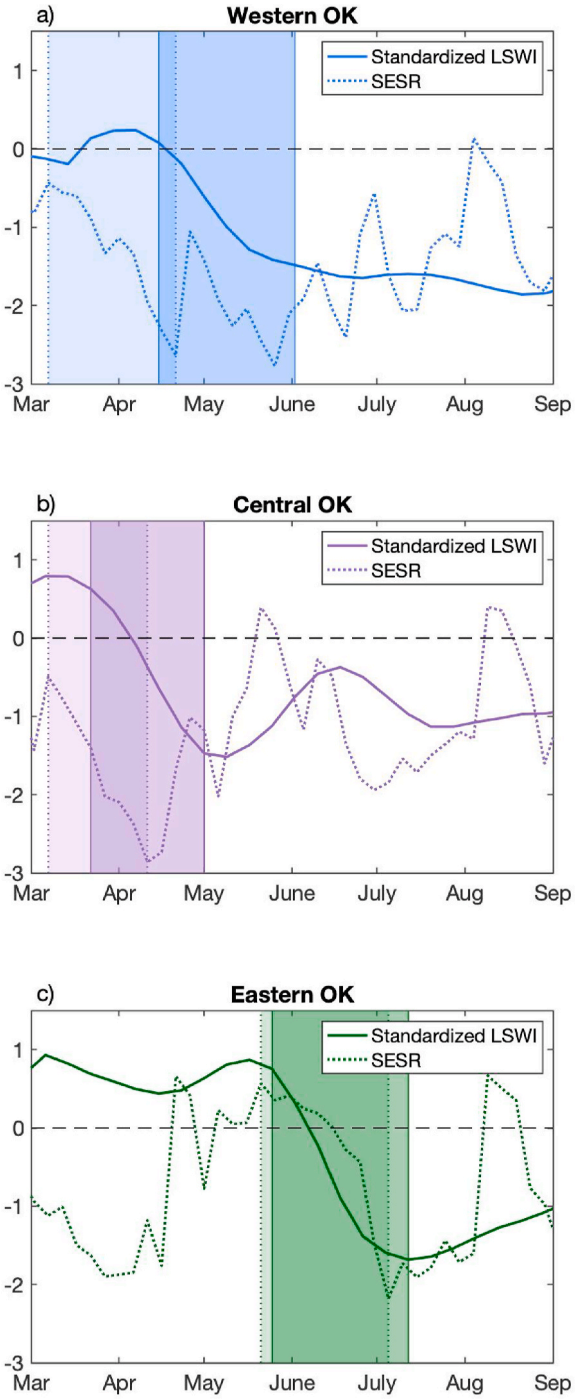

Fig. 6. Time series of standardized LSWI and SESR during the growing season for 2011 for a grid cell in a) western Oklahoma, b) central Oklahoma, and c) eastern Oklahoma. The darker shaded regions indicate the timing of flash drought depicted by FD_LSWI, while the lighter shaded regions indicate flash drought depicted by FD_SESR. Location of grid cells are indicated on Fig. 8.

3. Results

3.1. Temporal analysis of flash drought development

To examine the temporal evolution of flash drought identified by both FD_LSWI and FD_SESR during the growing season, three NARR grid cells were selected across Oklahoma for 2011 and 2012 (Figs. 6 and 7). These grid cells represent samples from different onset timings of rapid drought across Oklahoma. Further, the grid cells were chosen to coincide with locations where (1) FD_SESR was

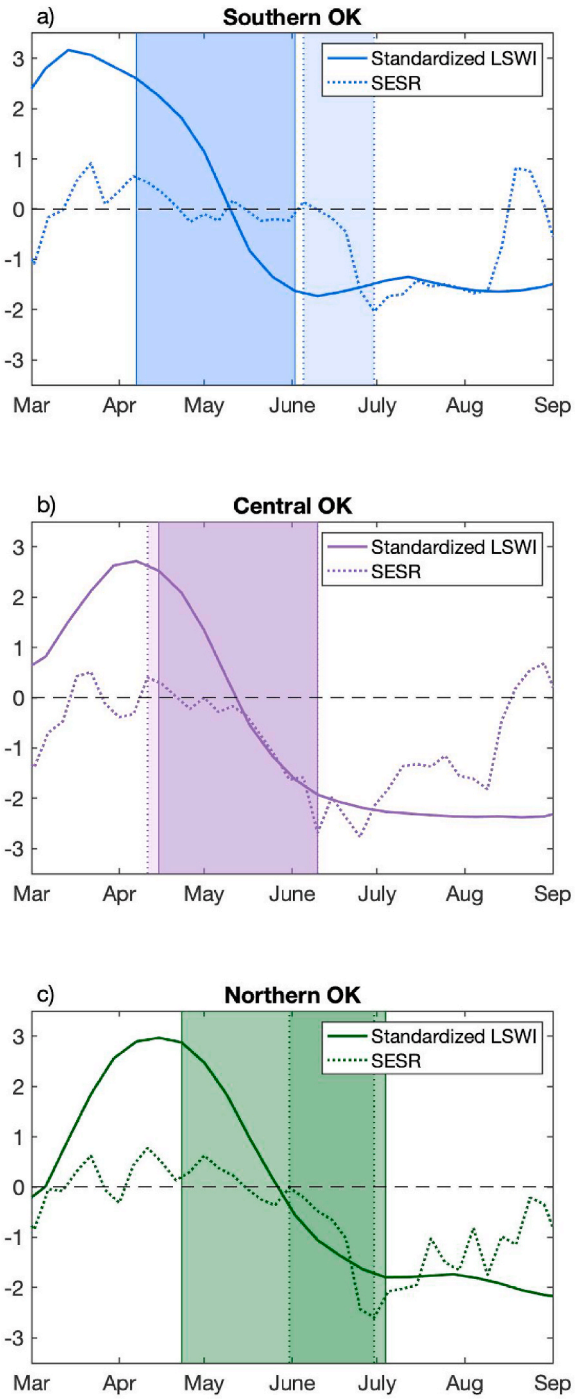

Fig. 7. Time series of standardized LSWI and SESR during the growing season for 2012 for a grid cell in a) southern Oklahoma, b) central Oklahoma, and c) northern Oklahoma. The darker shaded regions indicate the timing of flash drought depicted by FD_LSWI, while the lighter shaded regions indicate flash drought depicted by FD_SESR. Location of grid cells are indicated on Fig. 10.

identified and (2) a high density of pixels with FD_LSWI was identified (greater than 90% of land-based pixels identified with flash drought within the FD_SESR grid cell). Time-series of LSWI were produced by averaging standardized LSWI from all pixels with the modal start date within the grid cell. For the western, central, and eastern grid cells selected in 2011, the majority land cover type via MODIS is grasslands, croplands, and grasslands, respectively. For 2012, the southern grid cell has a majority land cover type of savannas, while the central and northern grid cells are primarily grasslands. In the NARR dataset, the three grid cells for 2011 and the three grid cells for 2012 are all classified as croplands.

Prior to flash drought development across Oklahoma in 2011, standardized LSWI was above-normal for each grid cell examined (Fig. 6). In contrast, SESR was below-normal for the western and central grid cells, and near-normal for the eastern grid cell. With respect to flash drought onset, LSWI first began to rapidly decline in central Oklahoma in late March (Fig. 6b). Rapid decreases in LSWI in western Oklahoma followed shortly thereafter with onset beginning in mid-April (Fig. 6a). Approximately 6–8 weeks after flash drought development began in central and western Oklahoma, onset of flash drought initiated at the eastern Oklahoma locations during late May (Fig. 6c). From the perspective of evaporative stress (SESR), flash drought began in early March for western and central Oklahoma, and mid-May for eastern Oklahoma. As such, FD_SESR onset emerged 1–5 weeks prior to onset derived by FD_LSWI for the grid cell locations. However, LSWI and SESR rapidly declined over the course of 4–6 weeks for all three locations and exhibited similar changes in magnitude for the standardized values.

For all three grid cells across Oklahoma in 2012, standardized LSWI was well above-normal with values between 2 and 3 standard deviation above the mean while SESR was slightly above-normal prior to flash drought development (Fig. 7). A notable result for the 2012 flash drought event was that the FD_LSWI onset of rapid drought intensification occurred 1–2 months prior to the rapid decrease in evaporative stress evident for the southern and northern Oklahoma grid cell (Fig. 7a,c). The exception was associated with the central Oklahoma grid cell, where SESR began to decrease approximately one week prior to a rapid decrease in standardized LSWI (Fig. 7b). Overall, the length of time associated with rapid drought development from FD_LSWI was approximately 8 weeks for each of the three grid cell locations, while FD_SESR was approximately 4 weeks for the southern and northern grid cell, and 8 weeks for the

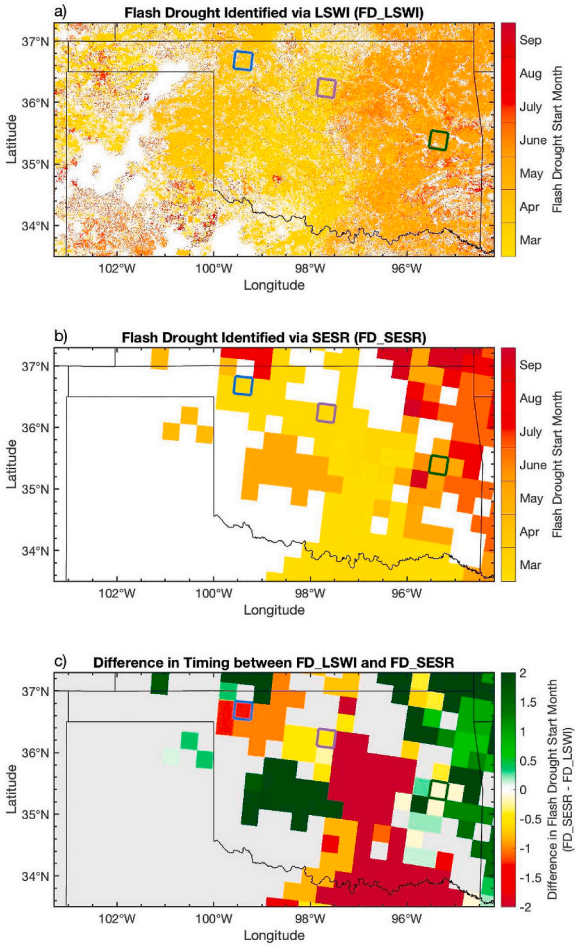

Fig. 8. a) Timing of flash drought via FD_LSWI, b) timing of flash drought via FD_SESR, and c) and the difference in flash drought start date depicted by FD_LSWI and FD_SESR for 2011. Gray grid cells indicate where flash drought was not identified from FD_LSWI or FD_SESR. The blue, purple, and green rectangles outline the grid cells used for analysis in Fig. 6. (For interpretation of the references to color in this figure legend, the reader is referred to the Web version of this article.)

central grid cell location.

3.2. Spatial analysis of flash drought development

To explore the spatial evolution of flash drought development, the month in which rapid drought intensification began was identified from FD_LSWI and FD_SESR (Fig. 8a and b). The difference in flash drought start month was also calculated by finding the modal start date of FD_LSWI flash drought from all pixels located in each NARR grid cell, then calculating the difference between the FD_SESR start date and the modal FD_LSWI start date (Fig. 8c). During 2011, FD_LSWI displayed expansive development of rapid drought intensification across most of Oklahoma (Fig. 8a). Further, flash drought initially developed in central Oklahoma during late March, with westward propagation during late April/early May and eastern progression of rapid drought development during late May/early June. Flash drought depicted by SESR displayed a spatiotemporal pattern similar to LSWI, with flash drought beginning in March across central Oklahoma along with further development in west-central and eastern Oklahoma during May and June (Fig. 8b). Overall, the start date for flash drought depicted by FD_SESR preceded the start from FD_LSWI across a large portion of Oklahoma,

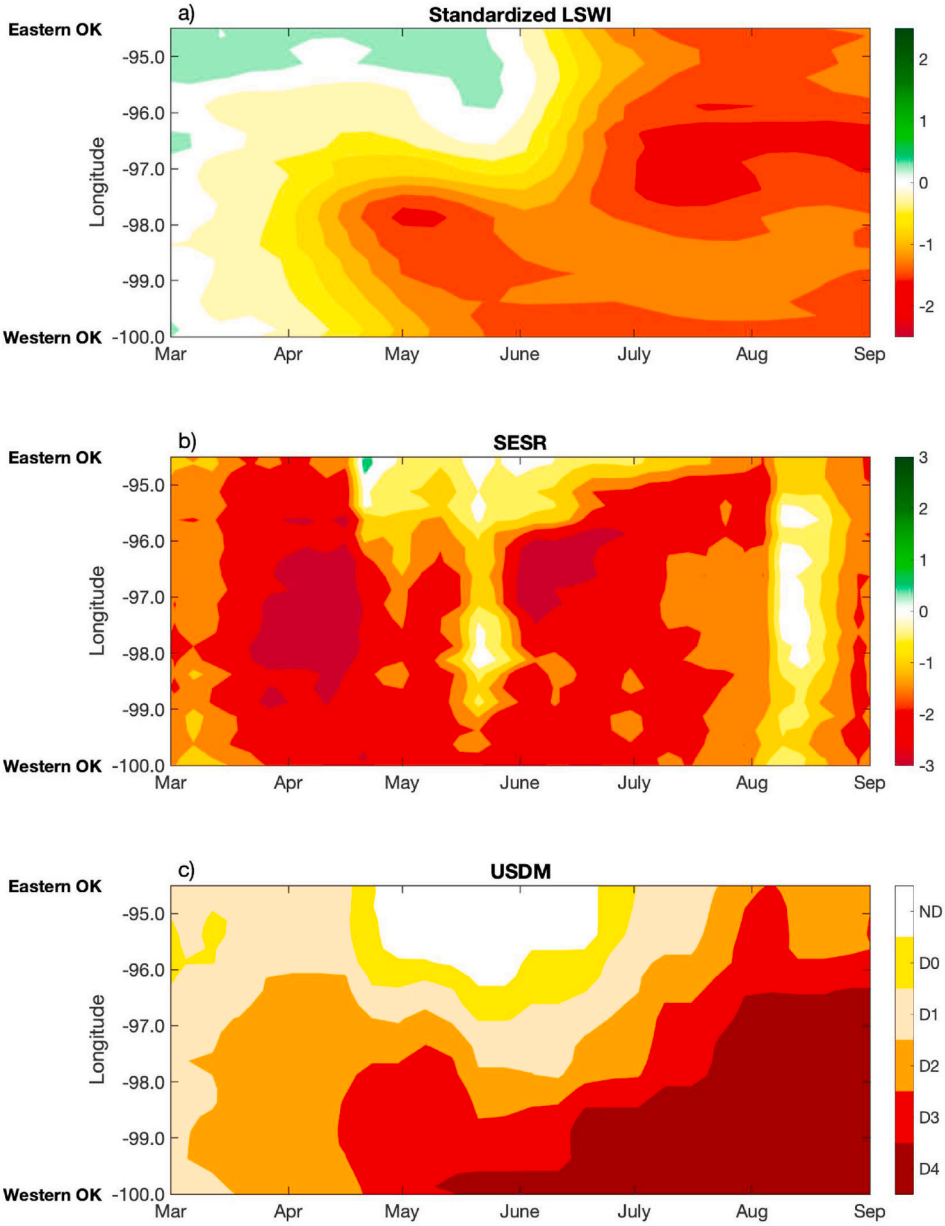

Fig. 9. Spatiotemporal evolution of (a) standardized LSWI, (b) SESR, and (c) the USDM during the growing season for 2011. Gradients in color shading oriented along the x-axis indicate a change in an index over time, while the spacing of the color shaded contours indicate the rate of change of an index over time (e.g., closer contours indicate a more rapid change in that index). (For interpretation of the references to color in this figure legend, the reader is referred to the Web version of this article.)

including the northwest, central, and southern areas of the state (Fig. 8c). However, FD_LSWI detected flash drought sooner than FD_SESR in west central Oklahoma and far eastern Oklahoma.

To illustrate the propagation of flash drought development, spatiotemporal plots of LSWI, SESR, and the USDM are provided in Fig. 9. For LSWI, SESR and the USDM, pixels and grid cells were averaged within 0.25° longitude swaths between 34°N and 37°N. The final USDM value for each swath was computed as the average drought monitor category (values of 0 through 4 used for D0-D4; −1 used for no drought). Flash drought development can be deduced by a strong negative gradient in values. Further, progression of flash drought development can be determined by the slope of individual contours, with steep/vertical slopes indicating concurrent development or rapid west/east propagation of drought, and relatively shallow slopes representing slower west/east propagation of drought.

Between 98.5 and 97.5°W (central Oklahoma), initial flash drought development occurred in LSWI with a negative gradient in LSWI values from late March to early May (Fig. 9a). The initial westward spread of flash drought is also evident from 98°W to 100°W. Eastward spread of flash drought (east of 97.5°W) began after D3 drought conditions were reached in central Oklahoma in May (Fig. 9c). However, flash drought developed mostly concurrently across eastern Oklahoma (indicated by the nearly vertical slope of the contours and Fig. 9a) and drought intensification was very rapid with a 1.5 decline in standardized LSWI in less than 4 weeks (on average) between 97 and 95°W (Fig. 9a).

SESR initially declined across the entirety of Oklahoma in March, but the greatest increase of evaporative stress is seen in central Oklahoma (98–96.5°W; Fig. 9b) similar to LSWI (Fig. 9a). However, the rapid decrease in SESR began in early March, approximately 3–4 weeks prior to decreases noted in the standardized LSWI. After a respite in evaporative stress across eastern Oklahoma (96.5–95°W) in late April and for a majority of Oklahoma in the middle of May (Fig. 9b), values of SESR declined very rapidly in eastern Oklahoma during late May which was followed by a rapid desiccation of vegetation and soil water content in early June (Fig. 9a).

The USDM indicated D1 and D2 drought across the majority of Oklahoma throughout March and early April (Fig. 9c). However,

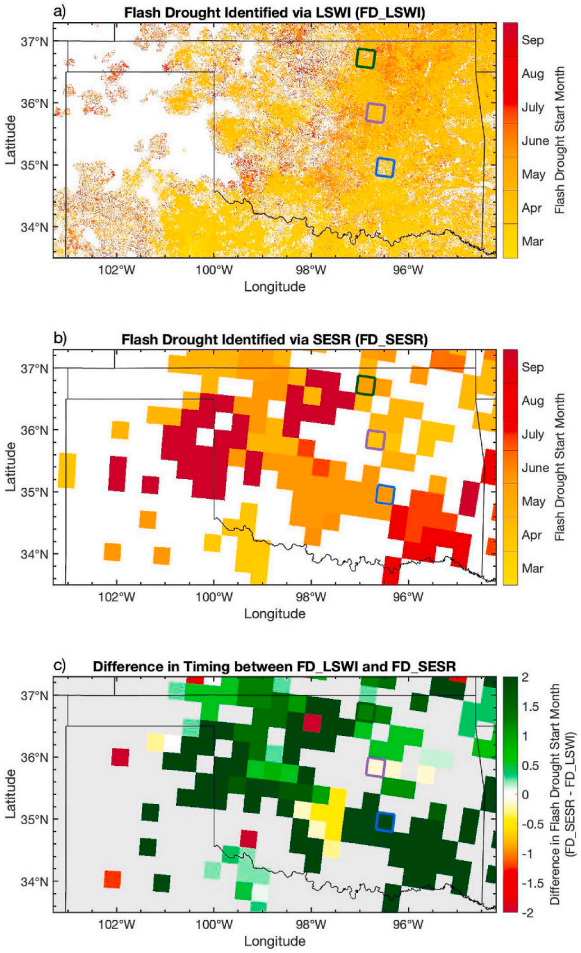

Fig. 10. a) Timing of flash drought via FD_LSWI, b) timing of flash drought via FD_SESR, and c) and the difference in flash drought start date depicted by FD_LSWI and FD_SESR for 2012. Gray grid cells indicate where flash drought was not identified from FD_LSWI or FD_SESR. The blue, purple, and green rectangles outline the grid cells used for analysis in Fig. 7. (For interpretation of the references to color in this figure legend, the reader is referred to the Web version of this article.)

unlike the central to western, then central to eastern progression of flash drought depicted by the standardized LSWI across Oklahoma, the USDM shows a continuous, relatively slow west-to-east progression of drought conditions. A two-category degradation of the USDM occurred in western Oklahoma between April and June, with a three-category degradation in central Oklahoma between early June and mid-July and eastern Oklahoma from mid-June to late July. Overall, declines in LSWI preceded drought intensification indicated from the USDM by 2–3 weeks.

For 2012, FD_LSWI shows rapid drought intensification occurring across most of Oklahoma with the exception of the Oklahoma panhandle (Fig. 10a). Further, desiccation of land surface conditions began in late March in southern Oklahoma, then rapidly propagated northward, with the onset of flash drought in mid-April in central Oklahoma and May in northern Oklahoma. The south-to-north progression of flash drought development is not evident via evaporative stress with FD_SESR yielding onset in April and May in northeast Oklahoma, June in south central Oklahoma, and latter portions of the growing season in local areas across southeast and northwest Oklahoma (Fig. 10b). Further, grid cells identified with FD_SESR were more sporadic across Oklahoma than FD_LSWI (Fig. 10a and b). Unlike 2011, FD_LSWI identified flash drought earlier than FD_SESR across a majority of Oklahoma in 2012, excluding a few grid cells in south central and east central Oklahoma (Fig. 10c).

Spatiotemporal plots of the 2012 flash drought across Oklahoma are shown in Fig. 11. To illustrate the south-to-north expansion of rapid drought intensification, 0.25° latitude swaths of LSWI, SESR, and the USDM were analyzed between 100 and 94.5°W from the southern to northern border of Oklahoma. The LSWI shows a rapid northward progression of flash drought development (Fig. 11a), similar to results found in Fig. 10a. Following the strongest gradient of contours (standardized LSWI from 1 to −1), rapid declines in LSWI began in early April at 34°N (southern Oklahoma) and mid-to late April around 37°N (northern Oklahoma). The slope of the gradient indicates that a 2–3 week lag existed for flash drought onset from south to north.

Results from SESR indicate a more complicated spatiotemporal pattern during the 2012 flash drought (Fig. 11b). During the rapid decline of LSWI in April, SESR remained near normal and did not begin to rapidly decline until June in central Oklahoma. After this time period, decreases in SESR expanded toward the southern and northern portions of Oklahoma, with the onset of flash drought lagging 2–3 weeks behind the timing of onset in central Oklahoma. Further, it is important to note that the time period of flash drought development depicted by SESR was temporally aligned with LSWI transitioning toward values that were well below average (Fig. 11a and b).

For most of the spring, the USDM indicated no drought conditions across a majority of Oklahoma (Fig. 11c). This was contemporaneous with well above average LSWI and near normal SESR between mid-March and late April. Abnormally dry conditions started to first appear in late May, then rapidly intensified toward D3 and D4 drought by early August. Similar to SESR, USDM did not identify

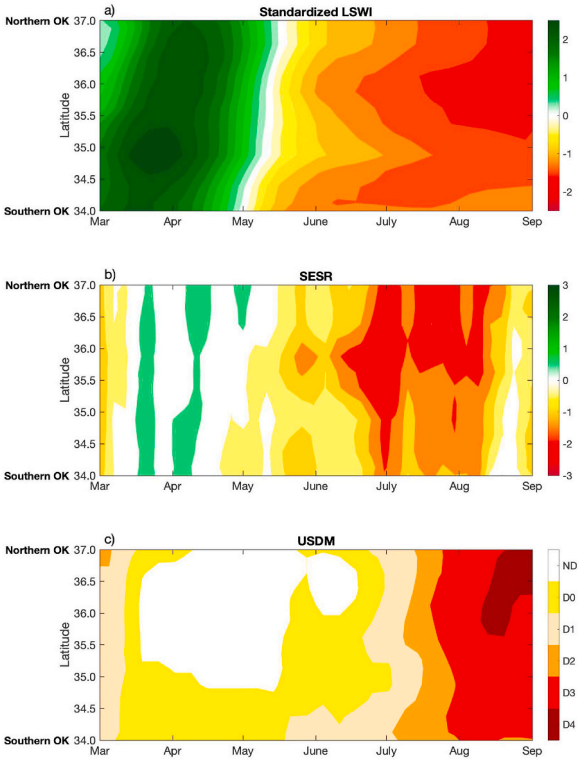

Fig. 11. Spatiotemporal evolution of (a) standardized LSWI, (b) SESR, and (c) the USDM during the growing season for 2012. Gradients in color shading oriented along the x-axis indicate a change in an index over time, while the spacing of the color shaded contours indicate the rate of change of an index over time (e.g., closer contours indicate a more rapid change in that index). (For interpretation of the references to color in this figure legend, the reader is referred to the Web version of this article.)

drought conditions until standardized LSWI decreased below 0 and reached D1 conditions in central and far southern Oklahoma approximately 1–2 weeks before the northern portion of Oklahoma. However, the slightly non-vertical slope of the contours between D0 and D2 indicate a rapid progression of drought conditions from central Oklahoma (35.5°N) to northern Oklahoma (36.5–37°N).

4. Discussion

4.1. Utility of FD_LSWI for flash drought identification

With over two decades of MODIS data, a novel opportunity is available to analyze flash drought development using satellite remote sensing observations from a climatological perspective as many flash drought identification methodologies use percentile-based approaches for flash drought detection (Christian et al., 2019a; Ford and Labosier, 2017; Osman et al., 2021; Yuan et al., 2019). As such, a sufficiently long dataset is required to increase percentile resolution for analysis. The 20 years of MODIS data provides a 5-percentile resolution for each 8-day period, which is adequate to delineate percentiles that meet the flash drought criteria in a modified identification framework via the FD_SESR methodology. Given this period of record for MODIS, an objective analysis of flash drought using satellite observations is possible for the first time within the scientific literature.

In this study, FD_LSWI was shown to represent flash drought development for case studies across Oklahoma during 2011 and 2012. Preexisting drought conditions were evident in the winter of 2011 with a majority of Oklahoma in D1 and D2 drought by early March (Fig. 12). In addition, the growing season during 2011 was much drier and warmer than usual (Tadesse et al., 2015; Tian and Quiring 2019) which increased the likelihood of flash drought development (Otkin et al., 2013). Following the dry winter period, FD_LSWI identified flash drought development in three distinct areas and timeframes. Central Oklahoma was the first area to undergo rapid drought intensification in late March and expanded upon longer term drought from western Oklahoma (Figs. 8a and 9c). Afterward, flash drought onset occurred across western Oklahoma in April and eastern Oklahoma in late May (Fig. 8a). The development of flash drought in three separate clusters can be loosely inferred from evaporative stress derived from a combination of land surface and atmospheric conditions (Fig. 8b) but is much more evident in the land-surface moisture-based LSWI (Fig. 8a). As such, approaches for flash drought detection using vegetation indices may provide a clearer spatial evolution of flash drought development from an impact-based perspective compared to indices that incorporate atmospheric conditions (i.e., evaporative demand).

The 2012 event across the central United States was initially marked by temperatures that were well above normal during the late winter and early spring (Jin et al., 2019) and led to an early green-up of vegetation (Ault et al., 2013). This green-up is strongly evident in the LSWI across Oklahoma, with standardized LSWI values exceeding 2 standard deviations above the mean (Fig. 11a). However, the early buildup of vegetation had consequences on the water cycle, with significant increases in evapotranspiration and rapid depletion of soil moisture (Wolf et al. 2016). While the impact of enhanced land surface desiccation is not observed with evaporative stress until June (Fig. 11b), the LSWI shows an early response in April indicating a reduction of vegetative and near surface moisture (Fig. 11a). Part of this early response is attributed to well above-average vegetative conditions in the early spring. Without exceptional amounts of rainfall to maintain the high positive anomaly in vegetation, a portion of time associated with the rapid decrease in LSWI in April and early May is the response of vegetative conditions returning to a normal state with respect to climatology. However, the LSWI ultimately provided additional information about the risk of flash drought development given the increased requirement of precipitation and soil moisture needed to maintain the anomalous state of vegetation health.

In prior studies that investigated flash drought occurrence, datasets with coarser grids (e.g., 5 km–50 km) are generally used to identify regions with rapid drought development (Basara et al., 2019; Christian et al., 2020; Koster et al., 2019; Otkin and Coauthors, 2016; Zhang et al., 2018). However, LSWI and other high-resolution VIs may be better suited for investigating the drivers of flash drought development and propagation such as land-atmosphere interactions. For example, the LSWI could be used to explore the relationship between fine-scale flash drought development and sensible heat advection for the propagation of drought and flash drought characteristics (Schumacher et al., 2019). Further, utilizing LSWI or a similar VI with a high spatial resolution may provide a better understanding of the role of land-atmosphere coupling in flash drought development (Wakefield et al., 2019; Basara et al., 2019).

4.2. Evaluation of FD_LSWI with drought impact

In addition to capturing rapid drought development, two key characteristics of any metric used for flash drought analysis is the ability to 1) identify drought conditions and 2) provide early warning for impending drought. Overall, the desiccation of land surface

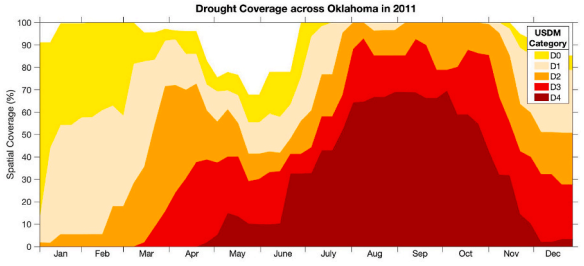

Fig. 12. The spatial coverage of the USDM categories across Oklahoma in 2011. Drought expanded and intensified in the early and middle portion of the growing season, with peak coverage and intensity in August and September.

conditions depicted by the LSWI aligns with drought conditions shown via the USDM for both the 2011 and 2012 case. In 2011, standardized LSWI values decreased from 0 to −1.5 across Oklahoma, with corresponding increases in USDM drought categories from D1 to D4 in western and central Oklahoma, and the absence of drought to D3 drought in eastern Oklahoma (Fig. 9a,c). Likewise, standardized LSWI values decreased from 2 to −1.5 for the 2012 flash drought event across Oklahoma (Fig. 11a). The USDM showed similar drought evolution, with land surface conditions deteriorating from no drought and D0 to D3/D4 across the state (Fig. 11c).

LSWI was also able to provide early warning for the rapid intensification toward drought conditions experienced across Oklahoma. For the 2011 event, flash drought development in central and western Oklahoma corresponded with the increasing spatial extent in drought conditions during the month of April (Figs. 8a and 12). However, flash drought development that occurred over the eastern third of land area across Oklahoma (Fig. 8a) is strongly evident, with rapid drought intensification in June preceding D4 drought conditions that developed across a majority of Oklahoma in by the end of July (Fig. 12). FD_LSWI also provided a notable lead time for drought development during the 2012 flash drought event (Fig. 13). Rapid drought intensification occurred during the months of April and May across Oklahoma as noted by the LSWI, but degradation in USDM categories did not begin until June and July (Figs. 10a and 13).

Overall, LSWI has not only been found to represent drought development and intensity (Bajgain et al., 2017, Wagle and Coauthors, 2014; Zhou and Coauthors, 2017, Figs. 9 and 11), but has also been shown in this study to have a high sensitivity to rapidly developing drought conditions (Figs. 6 and 7). As such, LSWI has the ability to depict drought and flash drought, and provide early warning for drought impacts identified via the USDM over Oklahoma. In addition, LSWI may have similar utility associated with flash drought identification over different land cover types in regions outside the Southern Great Plains, but future research is needed to explore the ability of the LSWI in flash drought depiction over other regions.

4.3. Comparison between FD_LSWI and FD_SESR

The spatial and temporal differences in flash drought identified via FD_LSWI and FD_SESR can be attributed to analysis technique and the fundamental drivers of LSWI and SESR. The first aspect is associated with the filtering technique applied to the LSWI time series. While LSWI was smoothed with the Savitzky-Golay filter, the SESR time series was unfiltered and has notable fluctuations between pentads (Figs. 6 and 7). These fluctuations are due to the fact that SESR is largely influenced by variables that can vary significantly from pentad-to-pentad (e.g., temperature, vapor pressure deficit, solar insolation). While moderation periods were included in the flash drought identification methodology for FD_SESR to account for these variations (Christian et al., 2019a), the methodology may be unable to capture flash drought in areas with large variations in SESR spanning multiple pentads, even if the overall trend of SESR is rapidly decreasing. As such, non-contiguous grid cells of flash drought identified with FD_SESR (Figs. 8b and 10b) may be associated with this variability and may be mitigated by smoothing the SESR time series with a filtering method such as the Savitzky-Golay filter.

Additionally, the timing of flash drought via FD_LSWI and FD_SESR often overlapped (Figs. 6 and 7). However, FD_LSWI generally detected flash drought onset before FD_SESR across Oklahoma in 2012 (Fig. 10c), while FD_SESR identified flash drought onset before FD_LSWI in 2011 (Fig. 8c). This difference can be attributed to the primary drivers of LSWI and SESR. LSWI represents the total water content in vegetation, and rapidly declining LSWI is indicative of deteriorating land surface conditions. In contrast, SESR is driven by the magnitude of ET and PET. ET corresponds to moisture at the land surface, while PET measures the atmospheric demand for surface-based moisture. In the case of 2011, the growing season was warmer than usual (Tadesse et al., 2015; Tian and Quiring 2019) such that flash drought was primarily driven by enhanced PET. An example of this is shown for the western Oklahoma grid cell (Fig. 14a). While vegetative conditions improved initially with enhanced PET (Fig. 6a; Fig. 14a), FD_SESR detected the initial PET increase as flash drought onset, providing early warning for flash drought with respect to FD_LSWI. The 2012 flash drought event across Oklahoma provides an example of when the decline of vegetation health is advantageous for flash drought early warning. With vegetative conditions well above-average during the spring (Fig. 7), ET was able to meet the atmospheric demand for moisture at the land surface (Fig. 14b) such that the ratio between ET and PET (SESR) remained near-normal through April and May (Fig. 7a). Only after vegetation conditions started to decline to values well below normal in June did PET start to rapidly increase with an associated decrease in ET. This resulted in flash drought identification via FD_SESR in June, while FD_LSWI, detected rapid drought intensification beginning in early April. While the results and analysis are limited to the response of LSWI in Oklahoma, FD_LSWI may be advantageous for early warning in flash drought monitoring, especially when vegetative conditions are above normal. This suggests the importance of

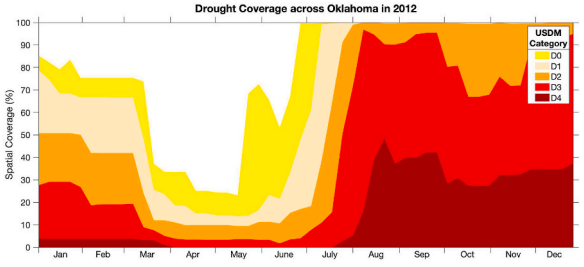

Fig. 13. The spatial coverage of the USDM categories across Oklahoma in 2012. Drought expanded and intensified in June and July, with peak coverage and intensity reached by August and September.

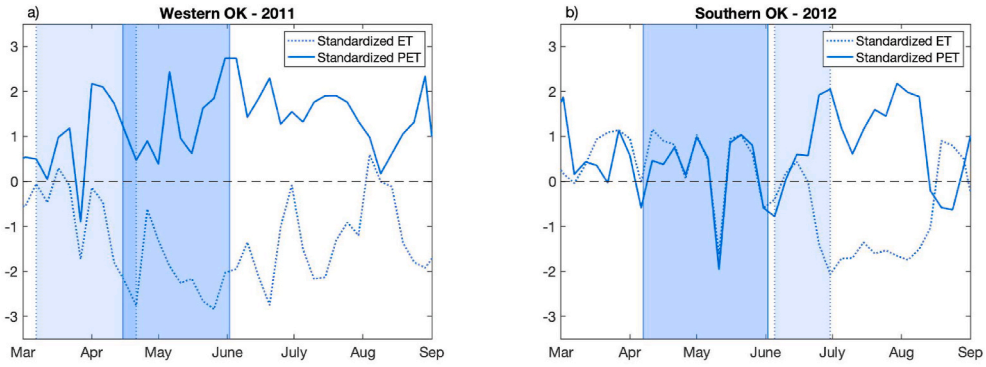

Fig. 14. Standardized ET and standardized PET from NARR for the western Oklahoma grid cell in 2011 (location of the grid cell on Fig. 8) and for the southern Oklahoma grid cell in 2012 (location of the grid cell on Fig. 10). The darker shaded regions indicate the timing of flash drought depicted by FD_LSWI, while the lighter shaded regions indicate flash drought depicted by FD_SESR.

considering vegetation and other land surface characteristics in flash drought detection and forecasting.

As an artifact of the smoothing procedure for LSWI using the Savitzky-Golay filter, it became possible to simplify the four criteria from the FD_SESR methodology. Specifically, the two criteria from FD_SESR that were used to capture rapid intensification (criteria 3 and 4) were reduced to a single criterion (criterion 3 in the updated methodology presented in this study). Overall, the smoothing procedure used for VIs not only allowed for a simplified flash drought identification methodology, but improved the ability to objectively capture flash drought by eliminating noise from the time-series. As such, using the Savitzky-Golay filtering technique in conjunction with the simplified methodology presents an updated version to the FD_SESR methodology. While the methodology presented in this study was used for a VI (LSWI), such an approach can also be used with other datasets and variables to improve flash drought identification.

4.4. Limitations

Some notable limitations exist in the analysis and when using satellite data with flash drought analysis. First, this study explores FD_LSWI for two case studies (2011 and 2012) over a relatively small area (the state of Oklahoma). While Oklahoma contains a diverse range of ecosystems and provided a solid foundation to explore the utility of FD_LSWI in flash drought identification, future work should further explore the ability of FD_LSWI across different geographic regions, land cover types, and climate regions. Second, this study compared FD_LSWI to evaporative stress derived flash drought from NARR and drought depicted by the USDM. Future research should compare FD_LSWI to other flash drought metrics/datasets and drought indicators to investigate FD_LSWI and its utility in flash drought monitoring and drought early warning.

Regarding satellite data, observations from satellite remote sensing are prone to missing data due to cloud coverage. While the procedure used in this study provided nearly 100% data coverage across Oklahoma, other geographic locations may have a higher frequency of cloud coverage. If data availability is not near 100% after an appropriate gap-filling technique is used, flash drought analysis may be hindered by clouds. However, cloud coverage and resulting cloud masks with MODIS data should be fairly limited in flash drought scenarios. This is fundamentally due to an increase in PET during flash drought development, which is often associated with increased solar insolation due to a lack of clouds. In addition to interpolation, Aqua MODIS data can be incorporated with the Terra MODIS data to increase the data availability. The second limitation is the inability to categorize flash droughts by their rate of intensification towards drought. A unique ability of some flash drought identification methodologies is to categorize the rate of intensification during flash drought (Christian et al., 2019a, Otkin and Coauthors, 2021), similar to how the USDM categorizes drought by severity (Svoboda and Coauthors, 2002). However, the accurate classification of flash drought intensity (rate of intensification) requires a higher resolution of percentiles, which is only possible once several decades of data are available from a given dataset. While intensity categorization was not possible in this study, percentile resolution will improve as the length of satellite observations progresses with time.

5. Conclusions

This study explored the utility of a satellite-based vegetation index (LSWI) for flash drought identification for two cases studies of rapid drought intensification across Oklahoma (the years 2011 and 2012). A critical result of this analysis was that FD_LSWI was able to depict the spatial and temporal evolution flash drought as an individual metric. Further, FD_LSWI was able to reveal spatial propagation of flash drought events not otherwise seen with coarser meteorological data (e.g., reanalysis data), and was able to provide early warning for drought conditions depicted by the USDM for two case studies across Oklahoma. Because LSWI yields information on vegetative water content such that land surface impact can be directly inferred from the index, LSWI has the ability to simultaneously quantify rapid drought intensification and represent drought conditions and provide a critically important perspective of flash drought development, in addition to other variables used for flash drought identification (e.g., evaporative stress and soil moisture).

Future work should continue to explore the utility of LSWI and other vegetation indices with flash drought identification. While the LSWI performed well in flash drought analysis with the primary land cover types in the localized study domain across Oklahoma (cultivated areas, grasslands, forests), further studies should examine the use of FD_LSWI over different regions. High-resolution flash drought identification derived from LSWI also expands research opportunities to explore fine-scale relationships between rapid drought intensification and land-atmosphere interactions. In addition, individual variables and metrics have unique benefits in flash drought identification (e.g., vegetation indices, evaporative stress, and soil moisture). However, composite indices should be investigated in future work to improve the identification of flash drought and enhance the lead time on rapidly deteriorating drought conditions.

Author contributions

J.I.C. conceived of the presented idea. J.I.C., J.B.B., and X.X. organized the outline. J.I.C. took the lead in writing the manuscript and provided figures. L.L. contributed to the development of the methodology. All authors contributed to the writing of the article.

Funding

This research was funded by National Science Foundation grants (OIA-1920946 and OIA-1946093), USDA NIFA grant (2016-68002-24967) and a cooperative agreement with the USDA Southern Great Plains Climate Hub.

Data availability statement

LSWI derived from MODIS surface reflectance is available at https://search.earthdata.nasa.gov/, SESR derived from NARR ET and PET is available at https://psl.noaa.gov/data/gridded/data.narr.monolevel.html, and USDM data is available at https://droughtmonitor.unl.edu/DmData/GISData.aspx.

Ethical statement

All ethical practices have been followed in relation to the development, writing, and publication of the manuscript entitled “Flash Drought Identification from Satellite-Based Land Surface Water Index”.

Author statement

Jordan I. Christian: Conceptualization, Methodology, Formal analysis, Writing – Original Draft, Visualization. Jeffrey B. Basara: Writing – Review and Editing, Supervision. Lauren E.L. Lowman: Methodology, Writing – Review and Editing. Xiangming Xiao: Writing – Review and Editing. Daniel Mesheske: Writing – Review and Editing. Yuting Zhou: Writing – Review and Editing.

Declaration of competing interest

The authors declare that they have no known competing financial interests or personal relationships that could have appeared to influence the work reported in this paper.

References

Anderson, M.C., Norman, J.M., Mecikalski, J.R., Otkin, J.A., Kustas, W.P., 2007a. A climatological study of evapotranspiration and moisture stress across the continental United States based on thermal remote sensing: 1. Model formulation. J. Geophys. Res. 112, 921. https://doi.org/10.1029/2006JD007506.

Anderson, M.C., Norman, J.M., Mecikalski, J.R., Otkin, J.A., Kustas, W.P., 2007b. A climatological study of evapotranspiration and moisture stress across the continental United States based on thermal remote sensing: 2. Surface moisture climatology. J. Geophys. Res. 112, 1100. https://doi.org/10.1029/2006JD007507.

Anderson, M.C., Hain, C., Otkin, J., Zhan, X., Mo, K., Svoboda, M., Wardlow, B., Pimstein, A., 2013. An intercomparison of drought indicators based on thermal remote sensing and NLDAS-2 simulations with U.S. Drought monitor classifications. J. Hydrometeorol. 14, 1035–1056. https://doi.org/10.1175/JHM-D-12-0140.1.

Ault, T.R., Henebry, G.M., de Beurs, K.M., Schwartz, M.D., Betancourt, J.L., Moore, D., 2013. The false spring of 2012, earliest in North American record. Eos, Trans. Am. Geophys. Union 94, 181–182. https://doi.org/10.1002/2013EO200001.

Bajgain, R., Xiao, X., Wagle, P., Basara, J., Zhou, Y., 2015. Sensitivity analysis of vegetation indices to drought over two tallgrass prairie sites. ISPRS J. Photogrammetry Remote Sens. 108, 151–160. https://doi.org/10.1016/j.isprsjprs.2015.07.004.

Bajgain, R., Xiao, X., Basara, J., Wagle, P., Zhou, Y., Zhang, Y., Mahan, H., 2017. Assessing agricultural drought in summer over Oklahoma Mesonet sites using the water-related vegetation index from MODIS. Int. J. Biometeorol. 377–390.

Basara, J.B., Maybourn, J.N., Peirano, C.M., Tate, J.E., Brown, P.J., Hoey, J.D., Smith, B.R., 2013. Drought and associated impacts in the Great plains of the United States—a Review. Int. J. Geosci. 72–81. https://doi.org/10.4236/ijg.2013.46A2009, 04.

Basara, J.B., Christian, J.I., Wakefield, R.A., Otkin, J.A., Hunt, E.H., Brown, D.P., 2019. The evolution, propagation, and spread of flash drought in the Central United States during 2012. Environ. Res. Lett. 14, 084025 https://doi.org/10.1088/1748-9326/ab2cc0.

Chandrasekar, K., Sai, M.V.R.S., Roy, P.S., Dwevedi, R.S., 2010. Land surface water index (LSWI) response to rainfall and NDVI using the MODIS vegetation index product. Int. J. Rem. Sens. https://doi.org/10.1080/01431160802575653.

Chandrasekara, K., Saia, M., Behera, G., 2011. Assessment of early season agricultural drought through land surface water index (LSWI) and soil water balance model. ISPRS-Int. Arch. Photogram. Rem. Sens. Spatial Inf. Sci. 3820, 50–55.

Chen, J., Jönsson, P., Tamura, M., Gu, Z., Matsuchita, B., Eklundh, L., 2004. A simple method for reconstructing a high-quality NDVI time-series data set based on the Savitzky–Golay filter. Rem. Sens. Environ. 91, 332–344. https://doi.org/10.1016/j.rse.2004.03.014.

Chen, L.G., Gottschalck, J., Hartman, A., Miskus, D., Tinker, R., Artusa, A., 2019. Flash drought characteristics based on U.S. Drought monitor. Atmosphere 10, 498. https://doi.org/10.3390/atmos10090498.

Christian, J.I., Basara, J.B., Otkin, J.A., Hunt, E.D., Wakefield, R.A., Flanagan, P.X., Xiao, X., 2019a. A methodology for flash drought identification: application of flash drought frequency across the United States. J. Hydrometeorol. 20, 833–846. https://doi.org/10.1175/JHM-D-18-0198.1.
Christian, J.I., Basara, J.B., Otkin, J.A., Hunt, E.D., 2019b. Regional characteristics of flash droughts across the United States. Environ. Res. Commun. 1, 125004. https://doi.org/10.1088/2515-7620/ab50ca.
Christian, J.I., Basara, J.B., Hunt, E.D., Otkin, J.A., Xiao, X., 2020. Flash drought development and cascading impacts associated with the 2010 Russian heatwave. Environ. Res. Lett. 15, 094078 https://doi.org/10.1088/1748-9326/ab9faf.
Christian, J.I., Basara, J.B., Hunt, E.D., Otkin, J.A., Furtado, J.C., Mishra, V., Xiao, X., Randall, R.M., 2021. Global distribution, trends, and drivers of flash drought occurrence. Nat. Commun. 12, 6330. https://doi.org/10.1038/s41467-021-26692-z.
Cihlar, J., Ly, H., Li, Z., Chen, J., Pokrant, H., Huang, F., 1997. Multitemporal, multichannel AVHRR data sets for land biosphere studies—artifacts and corrections. Rem. Sens. Environ. 60, 35–57. https://doi.org/10.1016/S0034-4257(96)00137-X.
DeAngelis, A.M., Wang, H., Koster, R.D., Schubert, S.D., Chang, Y., Marshak, J., 2020. Prediction skill of the 2012 U.S. Great plains flash drought in subseasonal experiment (SubX) models. J. Clim. 33, 6229–6253. https://doi.org/10.1175/JCLI-D-19-0863.1.
Dong, J., Coauthors, 2015. Comparison of four EVI-based models for estimating gross primary production of maize and soybean croplands and tallgrass prairie under severe drought. Rem. Sens. Environ. 162, 154–168. https://doi.org/10.1016/j.rse.2015.02.022.
Ford, T.W., Labosier, C.F., 2017. Meteorological conditions associated with the onset of flash drought in the Eastern United States. Agric. For. Meteorol. 247, 414–423. https://doi.org/10.1016/j.agrformet.2017.08.031.
Ford, T.W., McRoberts, D.B., Quiring, S.M., Hall, R.E., 2015. On the utility of in situ soil moisture observations for flash drought early warning in Oklahoma, USA. Geophys. Res. Lett. 42, 9790–9798. https://doi.org/10.1002/2015GL066600.
He, M., Kimball, J.S., Yi, Y., Running, S., Guan, K., Jensco, K., Maxwell, B., Maneta, M., 2019. Impacts of the 2017 flash drought in the US Northern plains informed by satellite-based evapotranspiration and solar-induced fluorescence. Environ. Res. Lett. 14, 074019 https://doi.org/10.1088/1748-9326/ab22c3.
Hobbins, M.T., Wood, A., McEvoy, D.J., Huntington, J.L., Morton, C., Anderson, M., Hain, C., 2016. The evaporative de-mand drought index. Part I: linking drought evolution to variations in evaporative demand. J. Hydrometeorol. 17, 1745–1761. https://doi.org/10.1175/JHM-D-15-0121.1.
Hoell, A., Coauthors, 2020. Lessons learned from the 2017 flash drought across the U.S. Northern Great Plains and Canadian Prairies. Bull. Am. Meteorol. Soc. 1–46. https://doi.org/10.1175/BAMS-D-19-0272.1.
Jin, C., Luo, X., Xiao, X., Dong, J., Li, X., Yang, J., Zhao, D., 2019. The 2012 flash drought threatened US midwest agroecosystems. Chin. Geogr. Sci. 29, 768–783. https://doi.org/10.1007/s11769-019-1066-7.
Koster, R.D., Wang, H., Mahanama, S.P., DeAngelis, A.M., Schubert, S.D., Mahanama, S.P., DeAngelis, A.M., 2019. Flash drought as captured by reanalysis data: disentangling the contributions of precipitation deficit and excess evapotranspiration. J. Hydrometeorol. 20, 1241–1258. https://doi.org/10.1175/JHM-D-18-0242.1.
Lisonbee, J., Woloszyn, M., Skumanich, M., 2021. Making sense of flash drought: definitions, indicators, and where we go from here. J. Appl. Serv. Climatol. 2021, 1–19. https://doi.org/10.46275/JOASC.2021.02.001.
Lowman, L.E.L., Barros, A.P., 2018. Predicting canopy biophysical properties and sensitivity of plant carbon uptake to water limitations with a coupled eco-hydrological framework. Ecol. Model. 372, 33–52. https://doi.org/10.1016/j.ecolmodel.2018.01.011.
McEvoy, D.J., Huntington, J.L., Hobbins, M.T., Wood, A., Morton, C., Anderson, M., Hain, C., 2016. The evaporative de-mand drought index. Part II: CONUS-wide assessment against common drought indicators. J. Hydrometeorol. 17, 1763–1779. https://doi.org/10.1175/JHM-D-15-0122.1.
Mesinger, F., Coauthors, 2006. North American regional reanalysis. Bull. Am. Meteorol. Soc. 87, 343–360. https://doi.org/10.1175/BAMS-87-3-343.
Nguyen, H., Wheeler, M.C., Otkin, J.A., Cowan, T., Frost, A., Stone, R., 2019. Using the evaporative stress index to monitor flash drought in Australia. Environ. Res. Lett. 14, 064016 https://doi.org/10.1088/1748-9326/ab2103.
Osman, M., Zaitchik, B.F., Badr, H.S., Christian, J.I., Tadesse, T., Otkin, J.A., Anderson, M.C., 2021. Flash drought onset over the contiguous United States: sensitivity of inventories and trends to quantitative definitions. Hydrol. Earth Syst. Sci. 25, 565–581. https://doi.org/10.5194/hess-25-565-2021.
Otkin, J.A., Coauthors, 2016. Assessing the evolution of soil moisture and vegetation conditions during the 2012 United States flash drought. Agric. For. Meteorol. 218-219, 230–242. https://doi.org/10.1016/j.agrformet.2015.12.065.
Otkin, J.A., Coauthors, 2021. Development of a flash drought intensity index. Atmosphere 12, 741. https://doi.org/10.3390/atmos12060741.
Otkin, J.A., Anderson, M.C., Hain, C., Mladenova, I.E., Basara, J.B., Svoboda, M., 2013. Examining rapid onset drought development using the thermal infrared–based evaporative stress index. J. Hydrometeorol. 14, 1057–1074. https://doi.org/10.1175/JHM-D-12-0144.1.
Otkin, J.A., Anderson, M.C., Hain, C., Svoboda, M., 2014. Examining the relationship between drought development and rapid changes in the evaporative stress index. J. Hydrometeorol. 15, 938–956. https://doi.org/10.1175/JHM-D-13-0110.1.
Otkin, J.A., Svoboda, M., Hunt, E.D., Ford, T.W., Anderson, M.C., Hain, C., Basara, J.B., 2018. Flash droughts: a Review and assessment of the challenges imposed by rapid-onset droughts in the United States. Bull. Am. Meteorol. Soc. 99, 911–919. https://doi.org/10.1175/BAMS-D-17-0149.1.
Pendergrass, A.G., Coauthors, 2020. Flash droughts present a new challenge for subseasonal-to-seasonal prediction. Nat. Clim. Change 10, 191–199. https://doi.org/10.1038/s41558-020-0709-0.
Savitzky, A., Golay, M.J.E., 1964. Smoothing and Differentiation of Data by Simplified Least Squares Procedures. Anal Chem 36, 1627–1639. https://doi.org/10.1021/ac60214a047.
Schumacher, D.L., Keune, J., van Heerwaarden, C.C., de Arellano, J.V.-G., Teuling, A.J., Miralles, D.G., 2019. Amplification of mega-heatwaves through heat torrents fuelled by upwind drought. Nat. Geosci. 12, 712–717. https://doi.org/10.1038/s41561-019-0431-6.
Svoboda, M., Coauthors, 2002. The drought monitor. Bull. Am. Meteorol. Soc. 83, 1181–1190. https://doi.org/10.1175/1520-0477(2002)083<1181:TDM>2.3.CO;2.
Tadesse, T., Wardlow, B.D., Brown, J.F., Svoboda, M.D., Hayes, M.J., Fuchs, B., Gutzmer, D., 2015. Assessing the vegetation condition impacts of the 2011 drought across the U.S. Southern Great plains using the vegetation drought response index (VegDRI). J. Appl. Meteorol. Climatol. 54, 153–169. https://doi.org/10.1175/JAMC-D-14-0048.1.
Tian, L., Quiring, S.M., 2019. Spatial and temporal patterns of drought in Oklahoma (1901–2014). Int. J. Climatol. 39, 3365–3378. https://doi.org/10.1002/joc.6026.
Tucker, C.J., 1980. Remote sensing of leaf water content in the near infrared. Rem. Sens. Environ. 10, 23–32. https://doi.org/10.1016/0034-4257(80)90096-6.
Wagle, P., Coauthors, 2014. Sensitivity of vegetation indices and gross primary production of tallgrass prairie to severe drought. Rem. Sens. Environ. 152, 1–14. https://doi.org/10.1016/j.rse.2014.05.010.
Wakefield, R.A., Basara, J.B., Furtado, J.C., Illston, B.G., Ferguson, C.R., Klein, P.M., 2019. A modified framework for quantifying land–atmosphere covariability during hydrometeorological and soil wetness extremes in Oklahoma. J. Appl. Meteorol. Climatol. 58, 1465–1483. https://doi.org/10.1175/JAMC-D-18-0230.1.
Wilhite, D.A., Svoboda, M.D., Hayes, M.J., 2007. Understanding the complex impacts of drought: a key to enhancing drought mitigation and preparedness. Water Resour. Manag. 21, 763–774. https://doi.org/10.1007/s11269-006-9076-5.
Wolf, S., Coauthors, 2016. Warm spring reduced carbon cycle impact of the 2012 US summer drought. Proc. Natl. Acad. Sci. Unit. States Am. 113, 5880–5885. https://doi.org/10.1073/pnas.1519620113.
Xiao, X., Boles, S., Frolking, S., Salas, W., Moore III, B., Li, C., He, L., Zhao, R., 2002. Observation of flooding and rice trans-planting of paddy rice fields at the site to landscape scales in China using VEGETATION sensor data. Int. J. Rem. Sens. 23, 3009–3022. https://doi.org/10.1080/01431160110107734.
Xiao, X., Zhang, Q., Braswell, B., Urbanski, S., Boles, S., Wofsy, S., Moore III, B., Ojima, D., 2004. Modeling gross primary production of temperate deciduous broadleaf forest using satellite images and climate data. Rem. Sens. Environ. 91, 256–270. https://doi.org/10.1016/j.rse.2004.03.010.
Xue, J., Su, B., 2017. Significant remote sensing vegetation indices: a Review of developments and applications. J. Sens. 2017 https://doi.org/10.1155/2017/1353691.
Yuan, X., Wang, L., Wu, P., Ji, P., Sheffield, J., Zhang, M., 2019. Anthropogenic shift towards higher risk of flash drought over China. Nat. Commun. 10, 1–8. https://doi.org/10.1038/s41467-019-12692-7.
Zhang, Y., Xiao, X., Wu, X., Zhou, S., Zhang, G., Qin, Y., Dong, J., 2017. A global moderate resolution dataset of gross primary production of vegetation for 2000–2016. Sci. Data 4, 1–13. https://doi.org/10.1038/sdata.2017.165.

Zhang, Y., You, Q., Chen, C., Ge, J., Adnan, M., 2018. Evaluation of downscaled CMIP5 coupled with VIC model for flash drought simulation in a humid subtropical basin, China. J. Clim. 31, 1075–1090. https://doi.org/10.1175/JCLI-D-17-0378.1.

Zhang, M., Yuan, X., Otkin, J.A., 2020. Remote sensing of the impact of flash drought events on terrestrial carbon dynamics over China. Carbon Bal. Manag. 15, 20. https://doi.org/10.1186/s13021-020-00156-1.

Zhou, Y., Coauthors, 2017. Quantifying agricultural drought in tallgrass prairie region in the U.S. Southern Great Plains through analysis of a water-related vegetation index from MODIS images. Agric. For. Meteorol. 246, 111–122. https://doi.org/10.1016/j.agrformet.2017.06.007.